

WL-TR-94-3064

FAILURE ANALYSIS FOR POLYCARBONATE
TRANSPARENCIES



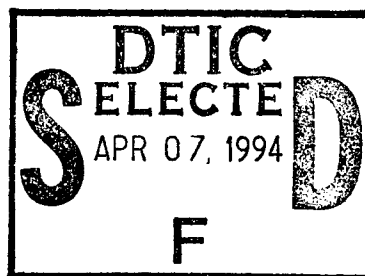
A. CHUDNOVSKY
T.J. CHEN
Z. ZHOU

DEPARTMENT OF CIVIL ENGINEERING
MECHANICS AND METALLURGY
UNIVERSITY OF ILLINOIS AT CHICAGO
CHICAGO IL 60680

C.P. BOSNYAK
K. SEHANOBISH

THE DOW CHEMICAL COMPANY
2301 N. BRAZOSPORT BLVD.
FREEPORT TX 77541-3257

MAY 1994



FINAL REPORT FOR 1 MAY 1994 THROUGH 1 SEPTEMBER 1994

APPROVED FOR PUBLIC RELEASE; DISTRIBUTION IS UNLIMITED.

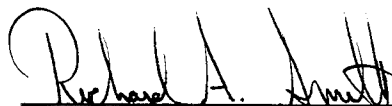
FLIGHT DYNAMICS DIRECTORATE
WRIGHT LABORATORY
AIR FORCE MATERIEL COMMAND
WRIGHT-PATTERSON AFB OH 45433-7562

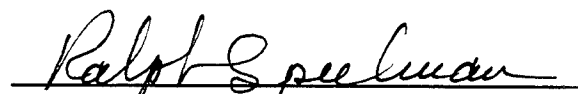
19950406 015

NOTICE

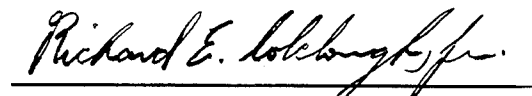
When Government drawings, specifications, or other data are used for any purpose other than in connection with a definitely Government-related procurement, the United States Government incurs no responsibility or any obligation whatsoever. The fact the government may have formulated or in any way supplied the said drawings, specifications, or other data, is not to be regarded by implication, or otherwise in any manner construed, as licensing the holder, or any other person or corporation; or as conveying any rights or permission to manufacture, use, or sell any patented invention that may in any way be related thereto.

This technical report has been reviewed and is approved for publication.


RICHARD A. SMITH
Aerospace Engineer


RALPH J. SPEELMAN III, Chief
Aircrew Protection Branch

FOR THE COMMANDER


RICHARD E. COLCLOUGH JR., Chief
Vehicle Subsystems Division

If your mailing address has been changed, if you wish to be removed from our mailing list, or if the addressee is no longer employed by your organization please notify WL/FIVR Bldg 255, 2079 10th St, WPAFB OH 45433-7502 to help us maintain a current mailing list.

Copies of this report should not be returned unless return is required by security considerations, contractual obligations, or notice on a specific document.

REPORT DOCUMENTATION PAGE			Form Approved OMB No. 0704-0188	
Public reporting burden for this collection of information is estimated to average 1 hour per response, including the time for reviewing instructions, searching existing data sources, gathering and maintaining the data needed, and completing and reviewing the collection of information. Send comments regarding this burden estimate or any other aspect of this collection of information, including suggestions for reducing this burden, to Washington Headquarters Services, Directorate for Information Operations and Reports, 1215 Jefferson Davis Highway, Suite 1204, Arlington, VA 22202-4302, and to the Office of Management and Budget, Paperwork Reduction Project (0704-0188), Washington, DC 20503.				
1. AGENCY USE ONLY (Leave blank)	2. REPORT DATE MAY 1994	3. REPORT TYPE AND DATES COVERED INTERIM 05/01/92--09/01/93		
4. TITLE AND SUBTITLE FAILURE ANALYSIS FOR POLYCARBONATE TRANSPARENCIES		5. FUNDING NUMBERS C F33615-92-C-3405 PE 62201 PR 2402 TA 03 WU TW		
6. AUTHOR(S) C. P. BOSNYAK K. SEHANOBISH				
7. PERFORMING ORGANIZATION NAME(S) AND ADDRESS(ES) DEPARTMENT OF CIVIL ENGINEERING MECHANICS AND METALLURGY UNIVERSITY OF ILLINOIS AT CHICAGO CHICAGO, IL 60680		8. PERFORMING ORGANIZATION REPORT NUMBER		
9. SPONSORING/MONITORING AGENCY NAME(S) AND ADDRESS(ES) FLIGHT DYNAMICS DIRECTORATE WRIGHT LABORATORY AIR FORCE MATERIEL COMMAND WRIGHT PATTERSON AFB OH 45433-7562		10. SPONSORING/MONITORING AGENCY REPORT NUMBER WL-TR-94-3064		
11. SUPPLEMENTARY NOTES				
12a. DISTRIBUTION / AVAILABILITY STATEMENT APPROVED FOR PUBLIC RELEASE; DISTRIBUTION IS UNLIMITED.		12b. DISTRIBUTION CODE		
13. ABSTRACT (Maximum 200 words) Today polymers are increasingly used in advanced structural applications such as aircraft canopies. However, there are no well established models which could be used by design engineers for predicting time to failure for these materials. Development of adequate criteria for three basic stages of fracture (crack initiation, stable crack growth and dynamic crack propagation) is necessary for the accurate prediction of service lifetime. Part 1 of this report reflects a recent progress in understanding of various failure initiation mechanisms in transparency-grade Polycarbonate (PC). A new fatigue crack initiation map for PC is proposed. Another important stage of the fracture process which may strongly influence the total lifetime is crack propagation. Propagation of a crack surrounded by the process zone is a well-known phenomenon for the PC. The properties of the material in the process zone may strongly influence such critical fracture parameters as lifetime, fracture toughness, etc. The deformation of PC by shear banding at a notch-tip was found very similar to that obtained by cold-drawing of PC. In the Part 2 of this report the tensile cold-drawing (necking) behavior of PC is further examined using simple tensile extension coupled with temperature measurements via an infrared camera.				
14. SUBJECT TERMS POLYCARBONATE, CRACK INITIATION, FRACTURE MECHANISM, COLD DRAWING, NECK, GLASS TRANSITION, TRUE STRESS		15. NUMBER OF PAGES 40		
		16. PRICE CODE		
17. SECURITY CLASSIFICATION OF REPORT UNCLASSIFIED	18. SECURITY CLASSIFICATION OF THIS PAGE UNCLASSIFIED	19. SECURITY CLASSIFICATION OF ABSTRACT UNCLASSIFIED	20. LIMITATION OF ABSTRACT UL	

LIST OF CONTENTS

INTRODUCTION	1
References	3

PART 1 A Fatigue Crack Initiation Mechanisms Map

1.1 Introduction	5
1.2 Experimental.....	6
1.2.1 Material and specimen preparation.....	6
1.2.2 Testing procedure.....	7
1.3 Results and discussion.....	7
1.4 Conclusions.....	21
1.5 References.....	22

PART 2 Cold Drawing (Necking) Behavior of Polycarbonate as a Double Glass Transition

2.1 Introduction	23
2.2 Experimental	24
2.3 Results	26
2.4 Discussion	36
2.5 Conclusions	39
2.6 References	39

Accession For	
NTIS CRA&I	<input checked="" type="checkbox"/>
DTIC TAB	<input type="checkbox"/>
Unannounced	<input type="checkbox"/>
Justification	
By	
Distribution /	
Availability Codes	
Dist	Avail and/or Special
A-1	

LIST OF FIGURES

Figure

1.1	Cooperative ductile fatigue failure initiation	8
1.2	Cooperative brittle fatigue failure initiation	9
1.3	Solo-crack brittle fatigue failure initiation	10
1.4	Mixed solo-crack brittle and cooperative ductile failure	11
1.5	Mixed cooperative brittle and cooperative ductile fatigue failure initiation	12
1.6	Thinning ratios at 0.2 mm surface crack length versus thickness	16
1.7	Number of fatigue cycles to initiate the 0.2 mm surface crack	17
1.8	σ_{\max}/σ_y versus $\log(N_i)$ for the various thicknesses	19
1.9	A fatigue crack initiation mechanism map for PC	20
2.1	Dumbbell specimen: a) Original material, b) Specimen cut from the drawn material	25
2.2	The engineering stress-strain response for polycarbonate, PC, at 23 °C at an initial strain rate of $3 \times 10^{-4} \text{ s}^{-1}$	26
2.3	The tensile behavior of the drawn PC	28
2.4	Strain rate dependency of yield, σ_y , and draw stress, σ_{dr} at 23 °C	29
2.5	Temperature dependence of σ_y and σ_{dr} at an initial strain rate	30
2.6	Temperature dependence of the transition strain	31
2.7	Temperature dependence of Young's modulus	31
2.8	Torsional dynamic mechanical analyses of the undrawn and drawn PC	32
2.9	Temperature dependence of the draw ratio λ_0	33
2.10	Temperature changes during the necking	34
2.11	Temperature changes on further stretching and unloading	35
2.12	The process of cold-drawing as transitions $\alpha \rightarrow \beta \rightarrow \gamma$	36

INTRODUCTION

Today polymers are increasingly used in advanced structural applications such as aircraft canopies. However, there are no well established models which could be used by design engineers for predicting time to failure for these materials, even under the simplest loading conditions. The large number of existing strength criteria reflects the lack of fundamental understanding of the conditions for failure. The basic progressive stages of failure can be considered as incubation leading to crack initiation, stable (controlled) crack growth and unstable (uncontrolled) crack propagation. Much effort has been placed in the fracture community towards the studies of crack propagation [1], but relatively little has been done on the crack initiation problem. Development of adequate criteria for all three basic stages of fracture is necessary for the accurate prediction of service lifetime. The relatively recent developments of failure mechanism maps dispel the naive concept of a single universal criterion for strength and represent the present level of understanding and characterization of strength of materials [2-5]. The axes usually chosen are applied stress normalized by the modulus and temperature normalized by either the melting point or the glass transition temperature. Using data from Bauwens-Crowet *et al.* [3] a fracture mechanism map for polycarbonate (PC) of Mw 35,000 g/mole in simple tension and compression for several strain rates and temperatures was developed by Bin Ahmed and Ashby [4]. Various regimes as elastic, plasticity and yielding, adiabatic heating, rubbery flow and viscous flow were identified. The main message gained from fracture mechanism maps is that there are various modes of fracture, each requiring its own failure criterion. Part 1 of this report reflects a recent progress in

understanding of various failure initiation mechanisms in PC. A new fatigue crack initiation map for PC is proposed.

Another important stage of the fracture process which may strongly influence the total lifetime is crack propagation. Propagation of a crack surrounded by the process zone is a well-known phenomenon for the PC. The studies have shown [6] that the properties of the material in the process zone may strongly influence such critical fracture parameters as lifetime, fracture toughness, etc. The importance of correlation between large deformations in thermoplastic polymers and their fracture behavior for engineering applications has been recognized by many researchers [7-11]. Poly(bisphenol A carbonate), PC, has received considerable attention because of its value as an impact resistant, transparent polymer with a glass transition temperature, T_g , around 150 °C. The characteristics of polycarbonate deformation around a notch or crack tip have been well studied and found to display various mechanisms dependent on the loading conditions and time under load [7, 8, 10, 12]. Shear banding predominates at short times and high loads, whereas microcracking occurs at low stresses and long times. The deformation of polycarbonate by shear banding at a notch-tip was found very similar to that obtained by cold-drawing of polycarbonate [7]. The phenomenology of tensile yield in PC has recently been reviewed by Stokes and Bushko [13] and the characteristics of tensile drawing of many polymers reviewed by Crist [14]. In the Part 2 of this report the tensile cold-drawing (necking) behavior of PC is further examined using simple tensile extension coupled with temperature measurements via an infrared camera.

REFERENCES

1. A. Moet, "Fatigue Behavior," *Failure of Plastics*, ed. by W. Brostow and R.D. Corneliussen, Hanser Publ., New York, Ch. 18, 1986.
2. M.F. Ashby, C. Gandhi and D.M.R. Taplin, *Acta Metallurgica*, Overview No. 3, **27** 699 (1979).
3. C. Bauwens-Crowet, J. C. Bauwens and G. A. Homes, *J. Mater. Sci.*, **7** 176 (1972).
4. Z. Bin Ahmad and M. F. Ashby, *J. Mater. Sci.*, **23** 2037 (1988).
5. M.T. Takemori, *Polym. Sci. and Eng.*, **28** 641 (1988).
6. A. Stojimirovic, K. Kadota and A. Chudnovsky, *J. Appl. Pol. Sci.*, **46** 1051 (1992)
7. A. Kim, L.V. Garret, C.P. Bosnyak and A. Chudnovsky, *J. Appl. Polym. Sci.*, **49** 877 (1993)
8. T-J Chen, C.P. Bosnyak, C-I. Kao, and A. Chudnovsky, *J. Appl. Polym. Sci.*, **49** 1909 (1993)
9. K. Kadota and A. Chudnovsky, *Polym. Eng. Sci.*, **32** 1097, (1992)
10. M. Ma, K. Vijayan, A.S. Hiltner and E. Baer, *J. Mater. Sci.*, **24** 2687 (1989)
11. R.N. Haward, *Macromolecules*, **26** 5860 (1993)
12. N. Verheulpen-Heymans and J.C. Bauwens, *J. Mater. Sci.*, **11** 1 (1976)
13. V.K. Stokes and W. C. Bushko in *Use of Plastics and Plastic Composites: Materials and Mechanics Issues*, V.K. Stokes, ed., pp 1-21, MD-Vol 46, American Society of Mechanical Engineers, New York, 1993

14. B. Crist, *Plastic Deformation of Polymers*, to be published in *Materials Science and Technology*, Volume 12, E.L. Thomas, ed.; VCH, Weinheim, Germany.

PART 1 A FATIGUE CRACK INITIATION MECHANISMS MAP

1.1 Introduction

Since the 1950's it became obvious that fracture toughness, defined as the resistance to crack initiation and growth, is another material property which is as important, if not more so, than strength for practical application. Fracture toughness is usually described in terms of a critical stress intensity factor, K_{Ic} , critical crack-tip opening displacement, CCTOD, critical energy release rate, G_{Ic} , J_{Ic} , etc. It is interesting to note the parallel of thought in the development of critical toughness criteria with those of critical strength criteria. Unfortunately, it appears the lessons gained from the evolution of strength criteria were not fully appreciated in the development of fracture toughness criteria. In both cases they have the same inherent limitations due to the lack of consideration of the effects of time. An example of a fatigue fracture mechanism map for plastics was developed by Takemori for an injection molded poly(bisphenol A carbonate), PC, a well-known tough engineering thermoplastic, of molecular weight, M_w 53,900 [1]. In these particular experiments the notch was introduced through the formation of a weldline and the tensile yield stress, σ_y , and glass transition temperature, T_g , were chosen for normalization. Three basic modes of failure were identified by Takemori for tension-tension fatigue of PC, (i) necking with applied stresses close to σ_y at a given temperature, (ii) shear banding at intermediate stresses and temperatures and (iii) crazing at low stresses and temperatures less than 70°C.

In this report we have begun the process of understanding failure initiation of a PC by first attempting to classify the various failure initiation

mechanisms available to this material in tension-tension fatigue. Here, we are determining the effects of varying stress level and thickness of PC using single-edge notched specimen. The range of thickness examined, 0.5 - 4.0 mm, was selected based on actual common utility of PC. We will show our first attempt at the development of a fatigue failure initiation mechanism map. We emphasize it leaves much room for further development through appropriate normalization of the axes.

1.2 EXPERIMENTAL

1.2.1 Material and Specimen Preparation

Polycarbonate, molecular weight, M_w 29,000 g/mole, was kindly provided by the Dow Chemical Company in the form of injection molded plaques of 3.1 and 6.2 mm thickness. After drying in a vacuum oven at 130°C for 24 hours, the plaques were further compressed to smaller thickness using a Dake Compression Molder under the following conditions: preheat 240°C under no load for 10 minutes, under 30 tons ram pressure for 20 minutes then cooled to 200°C by air followed by water to 30°C while still maintaining pressure. Rectangular specimens 80 mm x 20 mm were cut from the sheets and a 60° V-notch milled into the center of one long edge with notch length 1 mm and notch radius 0.01 mm. For tensile testing, dumbbell shaped specimens of gage length 50 mm x 10 mm were machined from the 3.1 mm plaques and pulled at an initial strain rate of 0.02% S⁻¹. The tensile yield stress, σ_y , was determined as 68 MPa. Generally three specimens were tested at each condition except with thickness 1.2 and 1.4 mm where at least 16 specimens were examined at σ_{max}/σ_y 0.45.

1.2.2 Testing procedure

The tension-tension fatigue experiments were conducted on a 1.1 ton capacity servohydraulic Instron Testing System at room temperature. Sinusoidal waveform loading with frequency 1.0 Hz was used for fatigue testing. The range of stress levels was (σ_{\max}/σ_y) 0.35 - 0.75 and minimum to maximum stress ratio, $R (\sigma_{\min}/\sigma_{\max}) = 0.4$.

The crack and surrounding damage was followed using a traveling optical microscope attached to a video camera. This assembly is equipped with a visual display unit from which the entire history of crack propagation is analyzed. Postfracture optical observations are performed on a Zeiss light microscope. For evaluation of the number of cycles to crack initiation, N_i , under the various conditions, the crack is considered to have initiated when it reached 0.2 mm from the notch on the specimen surface. This convention was adapted for ease of detection of the crack and hence consistency of measurement with duplicate specimens. The thinning ratio at a given crack length is defined as $(Z_0 - Z)/Z_0$ where Z_0 is the initial thickness and Z the fracture surface thickness.

1.3 Results and Discussion

In Figures 1.1-1.5 are shown the side view and fracture surfaces as viewed optically at 50X magnification of the various thickness specimens of polycarbonate subjected to 5 different loading conditions. From these pictures we can identify three basic mechanisms and two combinations of mechanisms. A typical example of *cooperative ductile* is seen in Figure 1.1, which is

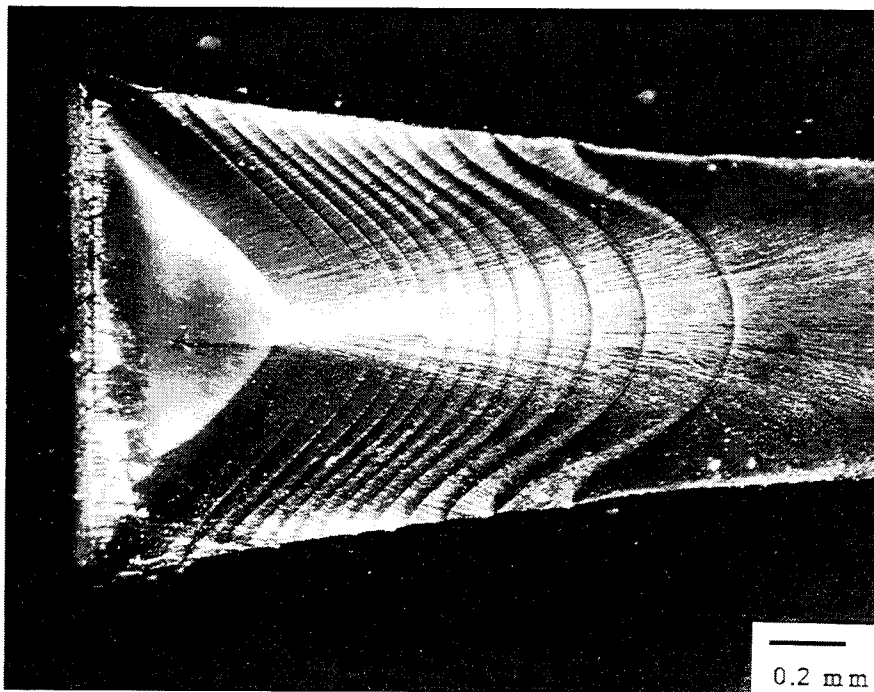
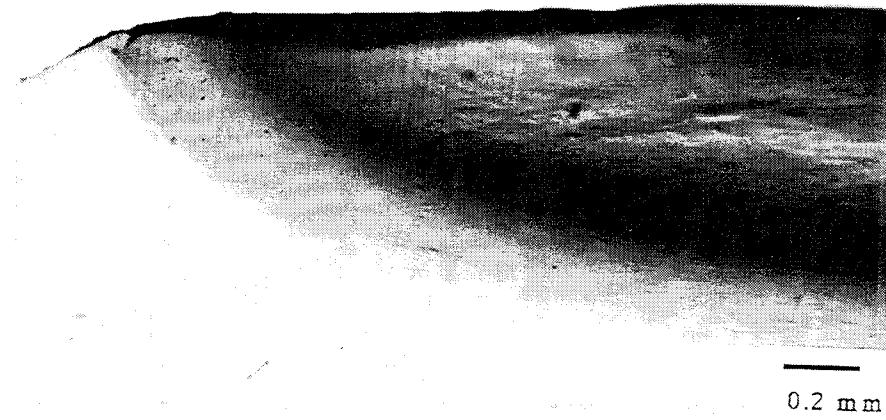


Figure 1.1 Cooperative ductile fatigue failure initiation in PC, $\sigma_{\max}/\sigma_y = 0.75$, thickness 1.4 mm.

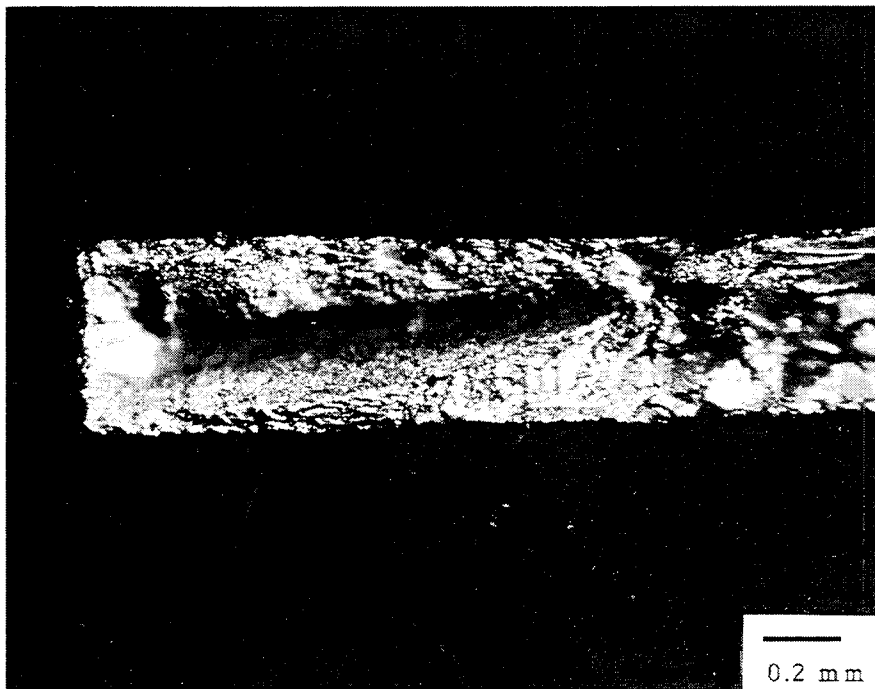
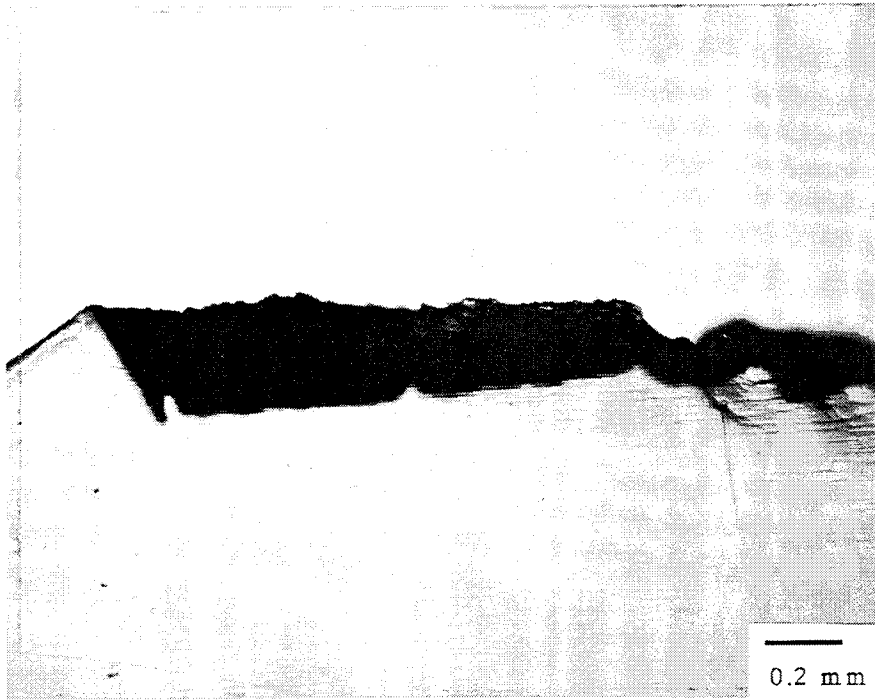


Figure 1.2 Cooperative brittle fatigue failure initiation in PC, $\sigma_{\max}/\sigma_y = 0.35$, thickness 0.5 mm.

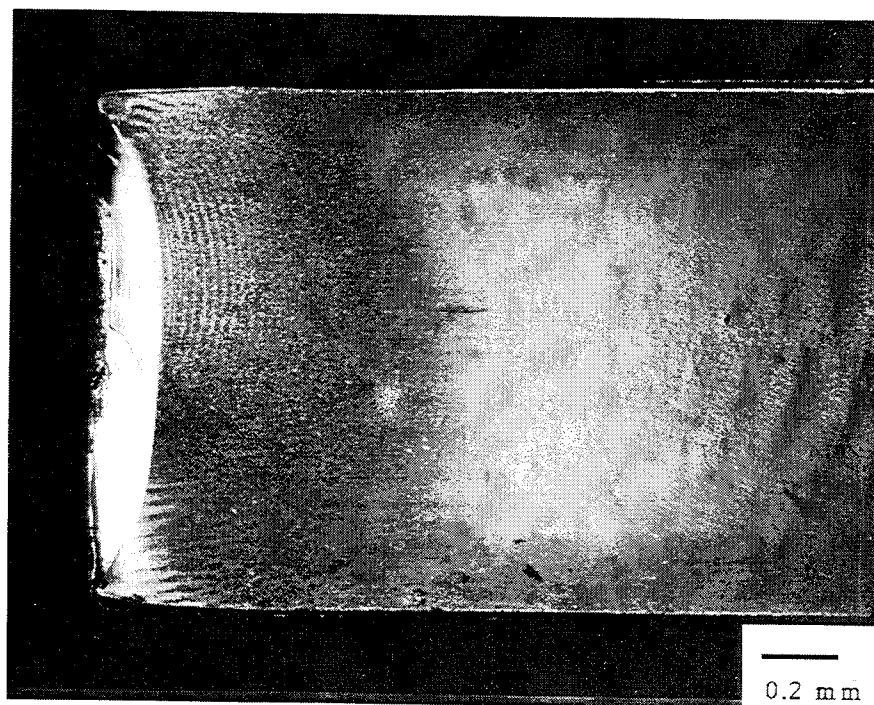
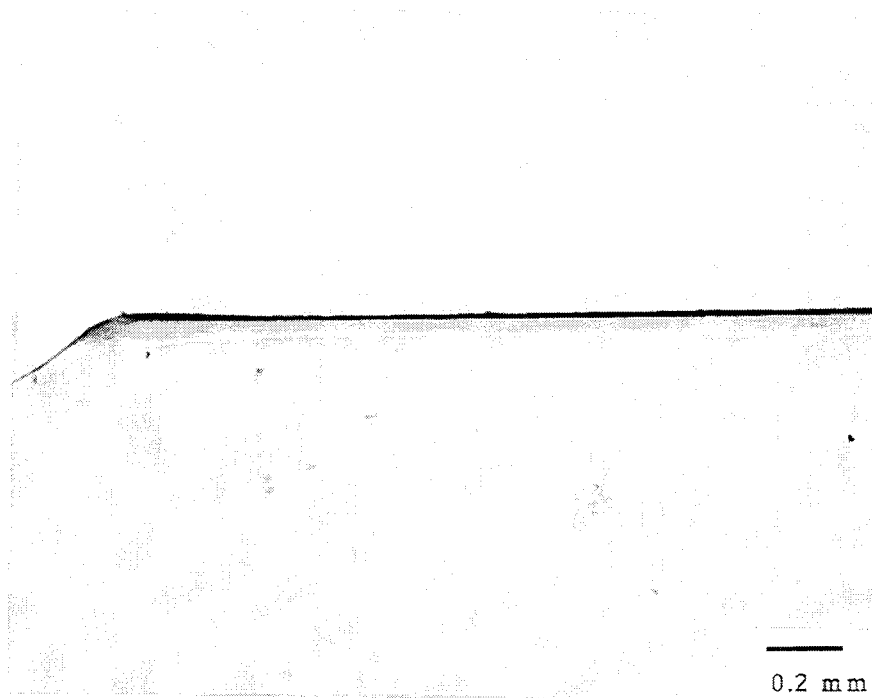


Figure 1.3 Solo-crack brittle fatigue failure initiation in PC, $\sigma_{\max}/\sigma_y = 0.45$, thickness 1.4 mm.

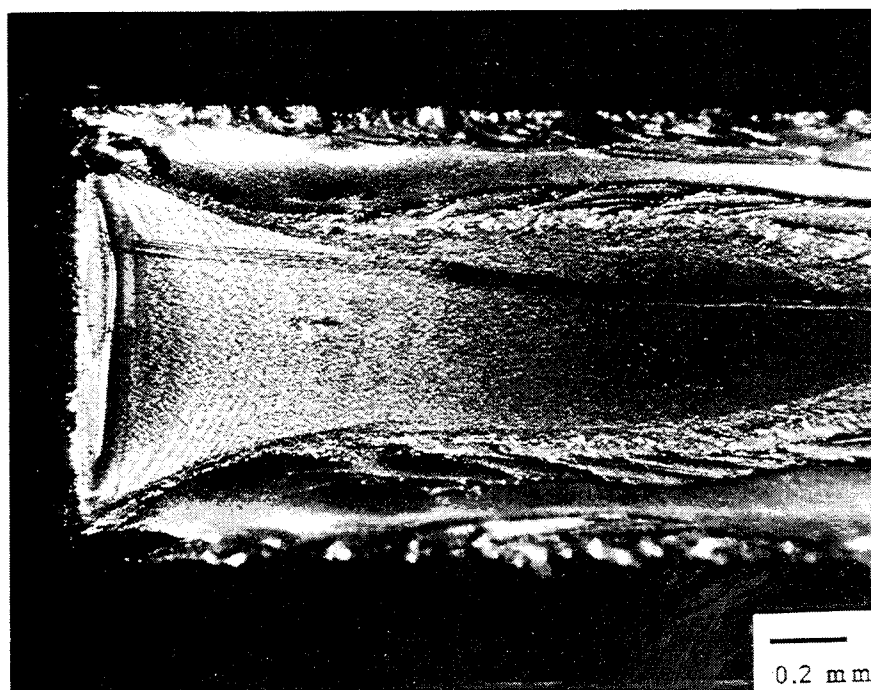
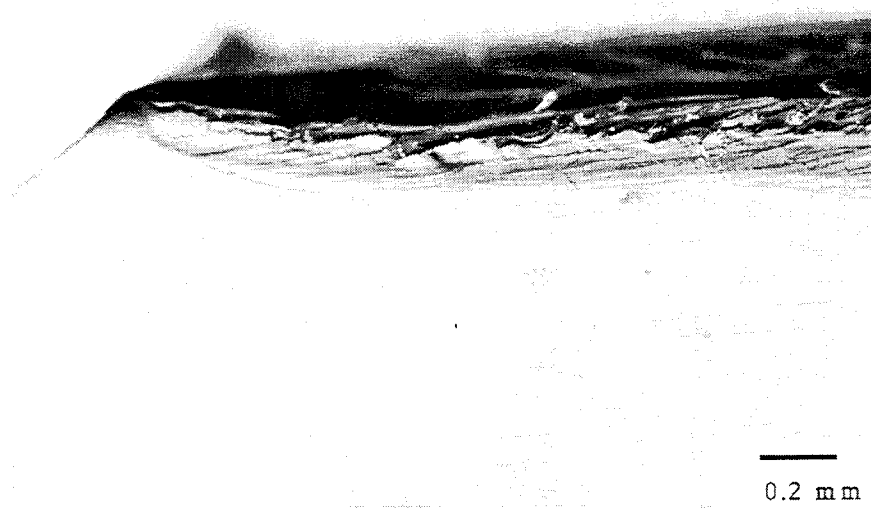


Figure 1.4 Mixed solo-crack brittle and cooperative ductile failure initiation in PC, $\sigma_{\max}/\sigma_y = 0.35$, thickness 1.2 mm.

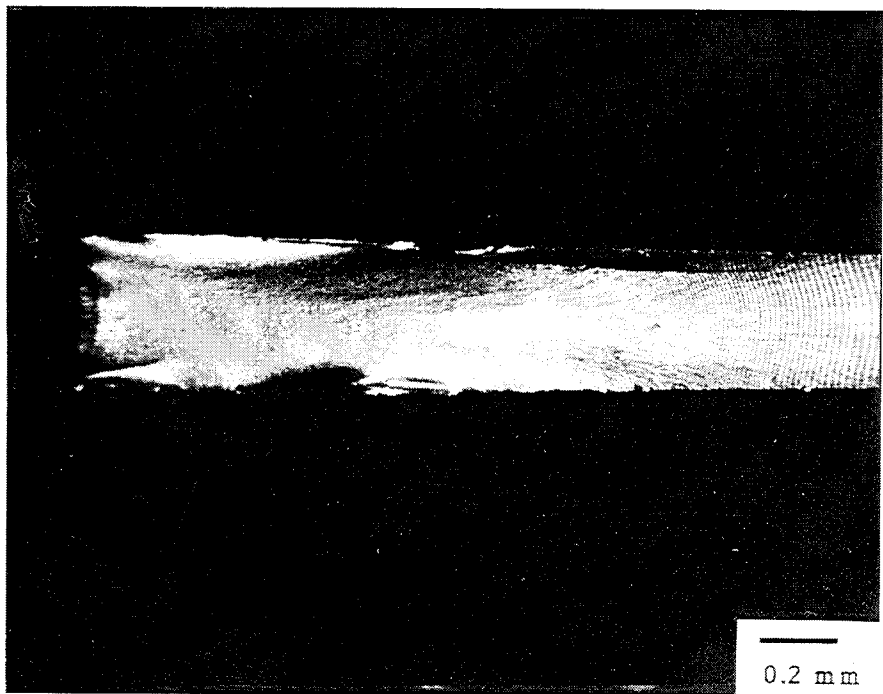
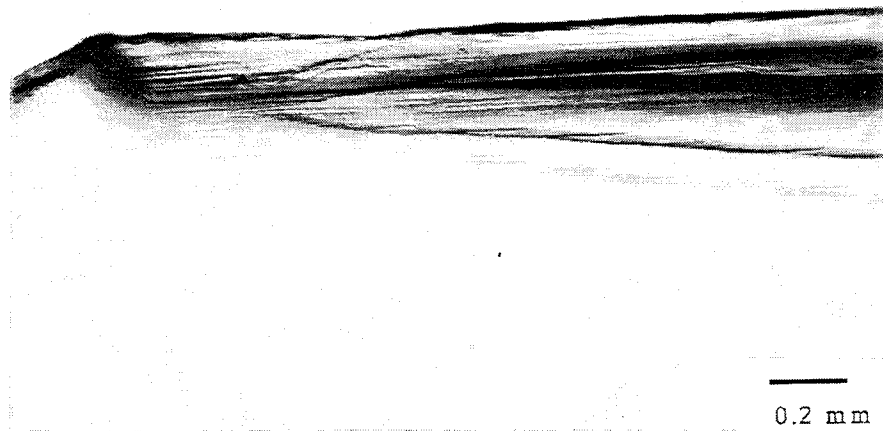


Figure 1.5 Mixed cooperative brittle and cooperative ductile fatigue failure initiation in PC, $\sigma_{\max}/\sigma_y = 0.55$, thickness 0.5 mm.

obtained at stress levels $\sigma_{\max}/\sigma_y > \sim 0.5$ for all thickness examined here.

The cooperative ductile mechanism is so named because the process zone associated with crack initiation consists of yielded material as reflected by a large thinning ratio and hence representative of significant cooperative deformation processes. This mechanism appears analogous to necking behavior in polycarbonate [1,2]. The crack grows through the midplane of the damage zone which is expected based on the symmetry of loading and geometry.

Figure 1.2 shows a representative fracture surface around the notch from the side and top view of specimens tested at $\sigma_{\max}/\sigma_y < 0.45$ and thicknesses, 0.5 - 1.0 mm. In spite of the symmetry of the loading and specimen geometry the process zone was observed to develop asymmetrically. Furthermore, the process zone apparently consists of a large number of microcracks or crazes and so we call the mechanism of initiation *cooperative brittle*. At this scale of magnification we were unable to determine whether these microfeatures were actually crazes as suggested by Takemori [1] or cracks, as described by Sehanobish *et al.* [3]. Some of this discrepancy could be ascribed to the effect of PC molecular weight; Takemori examined PC Mw 59,000, Sehanobish *et al.* 35,000 and ourselves 29,000 g/mole. Accordingly, we expect to be more similar to those observations by Sehanobish *et al.*, i.e., to develop microcracks. The microcracks were observed to develop along the lines expected of the principal stress trajectories. It was noted that in many cases the main crack did not grow initially through the midplane of the process zone, but also followed a curved path through the initially formed process zone before returning to the plane of the notch. The rough nature of the fracture surface seen in Figure 1.2 clearly indicates the main crack grew through a cloud of microcracks. We

suggest an important role is played by the statistics of critical defects which triggers the microcrack formation and subsequent crack initiation.

Figure 1.3 illustrates an example of a mechanism we have named *solo-crack brittle* at low stress levels $\sigma_{\max}/\sigma_y < 0.45$ and high thickness > 1.2 mm. Solo-crack brittle is a well-known failure mechanism of cross-linked polymers such as epoxies [4,5] with very little thinning. As the name suggests, only one crack is initiated which propagates immediately within one cycle to give ultimate part failure. Consequently, the surface is seen to be "mirror-like" with a very small process zone at the corners of the notch tip. In a manner similar to cooperative ductile, the crack grows through the plane of the notch tip.

Some of the mechanisms are seen to be competing with each other under certain intermediate conditions. For example, in Figure 1.4 are shown the side and top views of PC subjected to σ_{\max}/σ_y 0.35 and of thickness 1.0 mm. On the outer fracture surfaces of the specimen are observed the characteristics of cooperative brittle whereas in the core of the specimen a flat planar surface, solo-crack brittle, is seen. In contrast to the core fracture surface, the fracture surface of the sides of the specimen were not in the plane of the notch tip. There is little thinning of the specimen. Figure 1.5 illustrates an example of mixed cooperative-brittle and cooperative ductile failure at σ_{\max}/σ_y 0.55 and thickness 0.7 mm. Within about 0.15 mm of the notch tip are observed the dominant features of cooperative brittle. However, a struggle between the failure mechanisms is evident and thereafter ductile drawing is dominant.

The thinning ratios show the contribution of ductility in the specimens subjected to the various conditions. In Figure 1.6 are the thinning ratios (determined from the optical micrographs at 0.2 mm surface crack length) versus thickness of the PC for the stress levels examined. The reduction in ductility with decreasing stress level and increasing thickness is clearly seen.

These results are in good agreement with previous observations of the thinning ratio of various thickness PC tested in fatigue [3]. The increase in ductility with decreasing thickness is to be expected based on simple plane strain to plane stress considerations [6]. The thinning ratios are to be used in the future to quantify the energies involved in process zone evolution.

In Figure 1.7 is plotted the number of fatigue cycles to initiate the 0.2 mm surface crack, N_i , versus thickness of the sheets at the various stress levels examined. The error bars represent the scatter of N_i determined on 16 identical specimens. Generally the values of N_i at a given test condition were within a factor of 3. Some scatter in N_i with specimens of intermediate thicknesses arose from our method of determining crack growth from the surface because some crack tunneling was observed. From a general perspective, the values of N_i decrease with increase in thickness and increasing stress levels. Of importance, these results differ from those obtained with higher molecular weight PC (Mw 35,000 g/mole) where the values of N_i at $\sigma_{\max}/\sigma_y = 0.5$ increased with increasing thickness while maintaining a cooperative ductile failure mechanism [3]. The sensitivity of the failure mechanisms to PC molecular weight is well-known for impact failures [7] and several molecular weight PCs are presently being examined in fatigue in our laboratories.

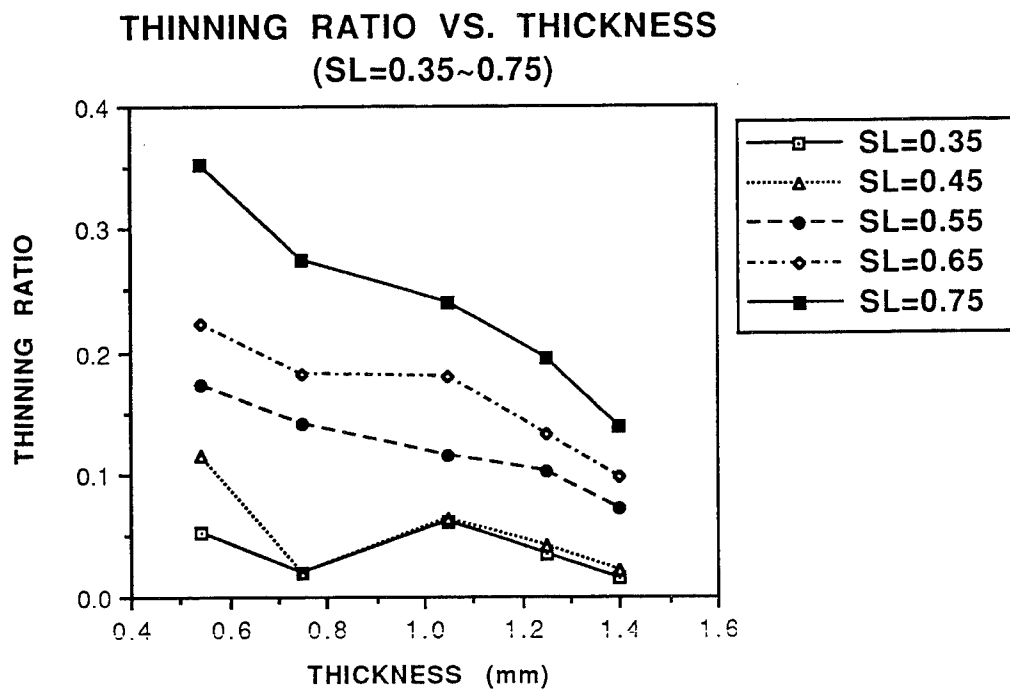


Figure 1.6 Thinning ratios at 0.2 mm surface crack length versus thickness of the PC for $\sigma_{\max}/\sigma_y = 0.35 - 0.75$.

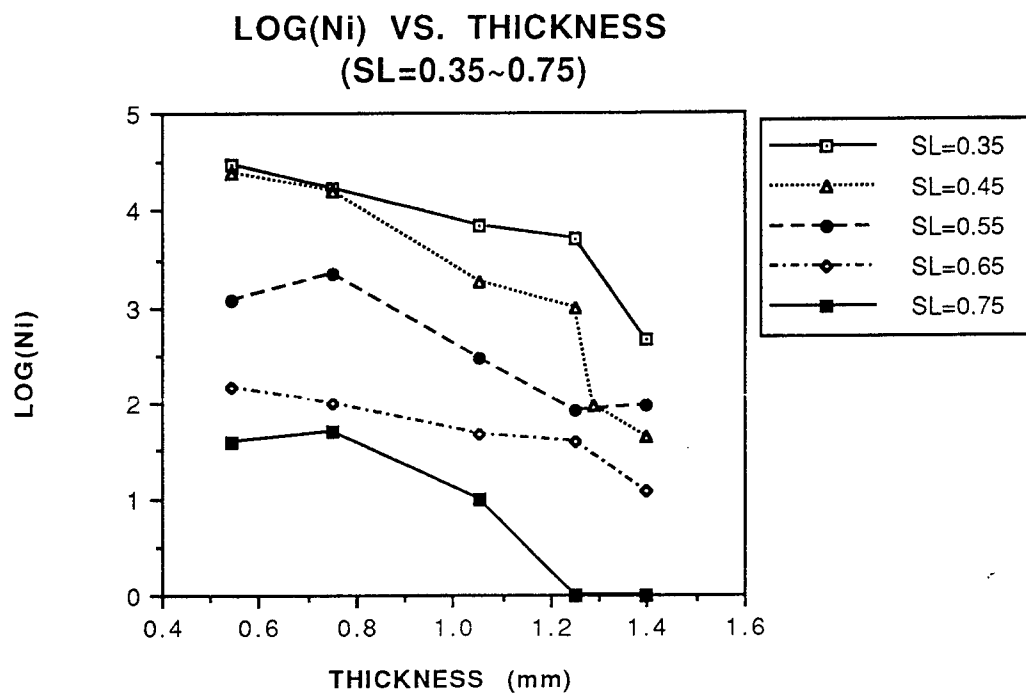


Figure 1.7 Number of fatigue cycles to initiate the 0.2 mm surface crack, N_i , versus thickness of the sheets at $\sigma_{\max}/\sigma_y = 0.35 - 0.75$.

It is useful to see the relationships between stress-level, the time to initiate a crack and the thickness of the sheet in regard to the failure mechanism. In Figure 1.8 is plotted the normalized applied stress versus $\log(N_i)$ for the various thicknesses denoted. The solid lines represent the connection of experimental data of the same failure initiation mechanism. The dashed lines represent the extension of a single mechanism and the dotted lines a transition in mechanism. To some extent this is similar to an approach taken by Takemori using total number of cycles to full part fracture [1]. Our observations are that the value of N_i for a given failure mechanism increases with decrease in applied stress and decreases with increasing sheet thickness. With thickness greater than 1.2 mm the number of cycles to initiate a crack underwent an inversion with decreasing stress levels at the point of change in mechanism from cooperative ductile to solo-crack brittle. The transition in initiation mechanisms from cooperative ductile to solo-crack brittle is very sudden with increasing thickness whereas transition from cooperative ductile to cooperative brittle is less well defined. This latter phenomenon is similar to that observed in fracture toughness evaluation of polycarbonate [7,8].

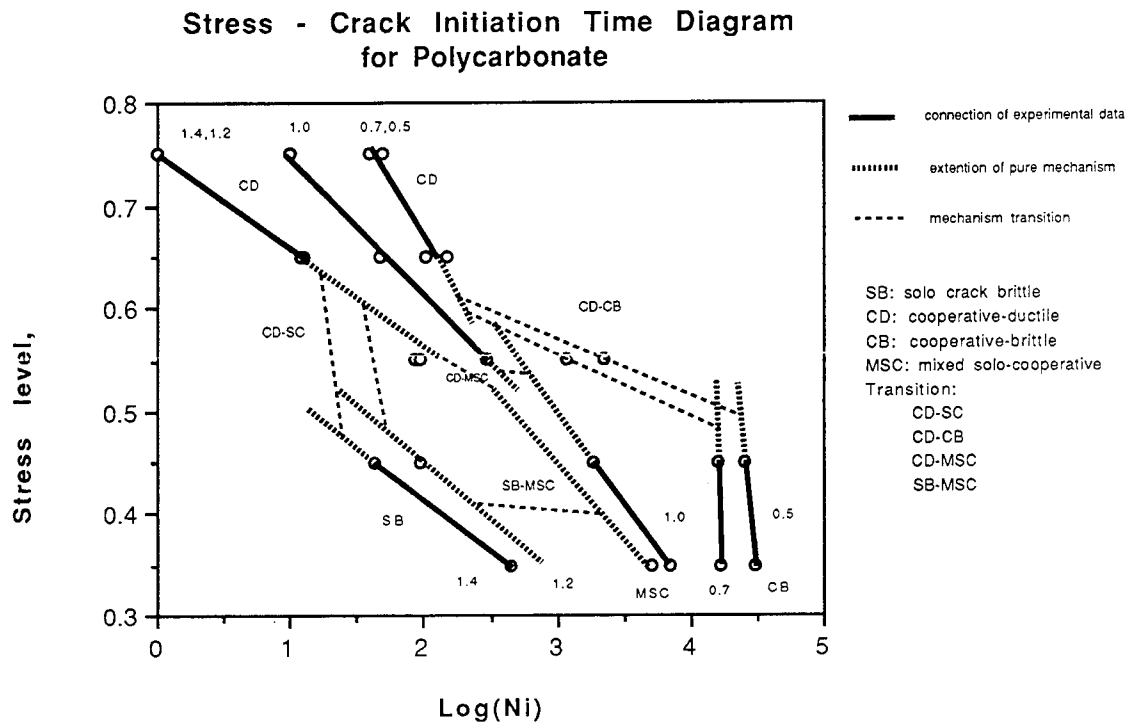


Figure 1.8 σ_{\max}/σ_y versus $\log(N_i)$ for the various thicknesses.

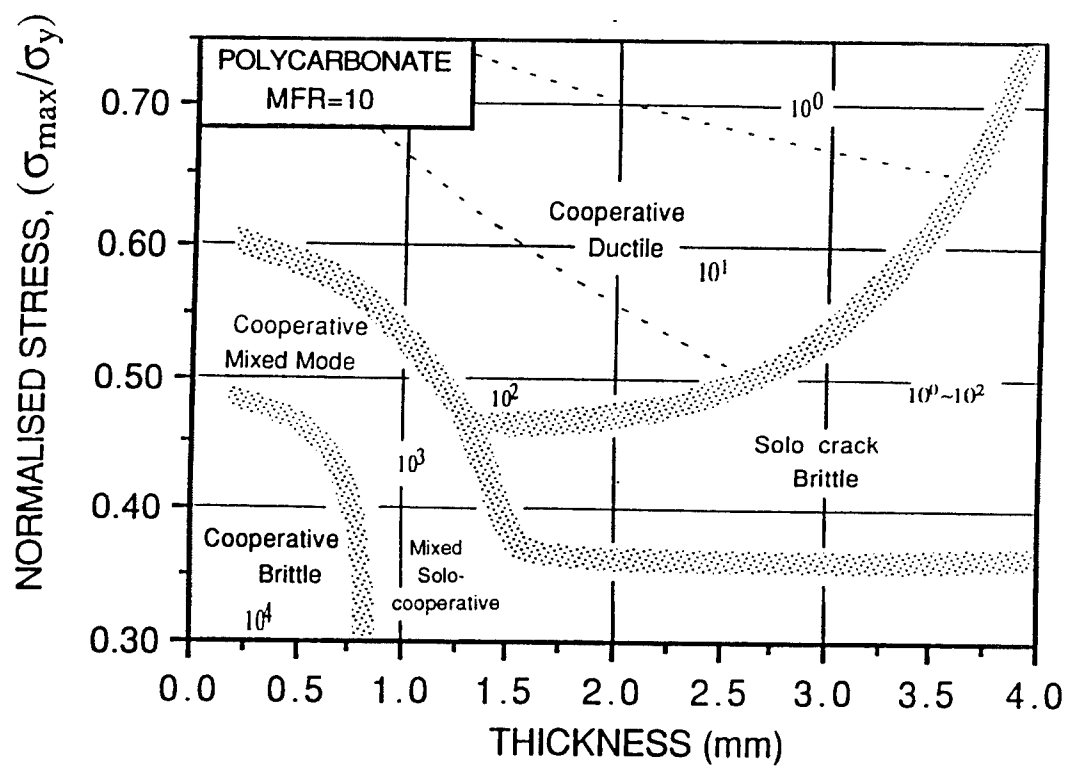


Figure 1.9 A fatigue crack initiation mechanism map for PC, Mw 29,000 g/mole.

In Figure 1.9 is given our first attempt of a fatigue crack initiation mechanism map for polycarbonate. The normalized applied stress is plotted against the thickness of the specimen. The orders of values of N_i are also shown in the plot. Attempts to use the stress intensity factor to normalize the loading conditions were made by changing the initial crack length from 1.0 mm to 0.5 and 2.0 mm. In some cases, the same initial values of the stress intensity gave different initiation mechanisms and so could not be used. As has been done elsewhere, the thickness of the sheet could be normalized against the plastic zone size calculated according to the well-known Dugdale-Barenblatt model [9]. However, this approach was also abandoned based on lack of additional knowledge it provided. It appears somewhat arbitrary in our case whether one selects the plastic zone size solution for plane stress or plane strain, the essential features of the map remain.

1.4 Conclusions

1. Novel fatigue crack initiation mechanisms maps are under development for engineering polymers. An illustrative example with polycarbonate is given where the effects of thickness (0.5 - 4 mm), and applied tensile loading at frequency 1 Hz on single-edge notched specimens are examined.
2. The number of fatigue cycles to initiate a crack were found strongly dependent on the micromechanism of deformation which occurs at the notch tip prior to crack formation and hence not to be a simple function of the applied stress.
3. Three basic fatigue crack initiation mechanisms were identified and named here as cooperative ductile, (at high stresses the damage zone formed

ahead of crack consisting of yielded material), solo-crack brittle (at large thicknesses very little damage zone development) and cooperative brittle, (identified as a cloud of microcracks that developed at the notch tip at low stresses in thin specimens). Increasing ductility was observed with decreasing thickness and applied stresses close to the tensile yield stress, but the change-over in mechanism with change in applied stress was much more dramatic for the thicker specimens.

1.5 References

1. Takemori, M.T.: Polymer fatigue fracture diagrams - BPA polycarbonate. Polym. Eng. Sci., 28: 641-647, 1988.
2. Ma. M., Vijayan, K., Hiltner, A. Bare, E. and Im, J.: Shear yielding modes of polycarbonate. J. Mater. Sci., 24: 2687-2696, 1989.
3. Shanobish, K., Haddaoui, N., and Moet, A.: Effect of thickness on ductile fatigue crack propagation in polycarbonate. J. Mater. Sci., 28: 1360-1366, 1993.
4. Kinloch, A. J. and Shaw, S. J.: Fracture resistance of a toughened epoxy adhesive. J. Adhes., 12: 59-77, 1981.
5. Chudnovsky, A., Kim, A., and Bosnyak, C.P.: Energy analysis of crack initiation and arrest in epoxy. Inter. J. Frac., 55: 209-220, 1992.
6. Knott, J. F., Fundamental of Fracture Mechanics, Butterworth, London, 1973.
7. Chang, F.-C. and Chu, L.-H.: Co-existence of ductile, semi-ductile, and brittle fracture of polycarbonate. J. Appl. polym. Sci., 44: 1615-1623, 1992.
8. Sehanobish, K., Bank, D.H., and Bosnyak, C.P.: Effect of geometric constraints on toughness of polycarbonate. J. Appl. Polym. Sci., to appera.
9. Parvin, M. and Williams, J.G.: Environmental craze growth in polycarbonate. Polym. Eng. Sci., 21: 816-821, 1981.

PART 2 Cold Drawing (Necking) Behavior of Polycarbonate as a Double Glass Transition

2.1 Introduction

Previous descriptions of the deformation of polycarbonate include "a deformation-induced van der Waals phase transition" by Muller [9], molecular-based interpretations such as the reduction of the T_g by the applied stress (or associated strain) [10-12], or breakdown of entanglements [13]. Each of these descriptions, however, have difficulties in accounting for the thermomechanical behavior on cold drawing of polymers [14]. Haward and Thackray [15] have attempted to describe the isothermal stress-strain behavior of ductile polymers using a mathematical model derived from a Hookean spring in series with an Eyring dashpot and rubber elasticity spring in parallel. The tendency for a polymer to show cold-drawing behavior was assumed to be related to the limiting strain, or the rubber elasticity component, of the polymer under the conditions of the test. More recently, Haward has examined the applicability of conventional rubber elasticity to true stress-strain behavior beyond the yield point and found that several crystalline polymers obey this relationship much below their melting point, but not polycarbonate [5]. Koenen et al. have discussed a phenomenological description of large deformations in polycarbonate using irreversible thermodynamics as a framework [16]. However, in their paper the physical characteristics of the cold-drawn state were not examined, which is considered an important omission and necessary to explain important features of the necking phenomena.

One objective of this study is to develop a consistent thermodynamic description for large-scale deformation of polycarbonate. The tensile behavior of the polycarbonate is examined in both the undrawn and drawn states as

functions of the temperature and the strain rate. A new construct which accounts for the features observed is then proposed. Based on observations by others, and by the authors, it is proposed that the necking phenomena is a special type of transformation involving double glass transitions, first from the isotropic glass to isotropic rubber at the yield point, then from the stretched rubber to the oriented glass upon unloading.

2.2 Experimental

Materials and Sample Preparation.

Polycarbonate samples with molecular weights of M_w 29,000 and 38,000 g/mole were provided by the Dow Chemical Company in the form of injection molded plaques of 3 mm thickness. After drying in a vacuum oven at 120 °C for 24 hours, the plaques were further compressed to various thicknesses in the range 0.2-1.3 mm using a Dake compression molder under the following conditions: preheat to 270 °C, hold at zero load for 10 minutes, compression under 4 MPa for 5 minutes, then another 8 minutes under this compression condition until cooled to 30 °C. Dumbbell tensile test specimens of the dimensions shown in Figure 2.1a were machined from the compression molded sheets. Smaller dumbbell specimens were machined from the necked portion of pulled specimens, Figure 2.1b.

Tensile Test.

The dumbbell specimens were marked with regularly spaced lines across the width and pulled with initial strain rates in the range from 3×10^{-4} to 3.0 s^{-1} and at temperatures in the range of 23-115 °C (± 0.5 °C) in a temperature controlled oven mounted on an Instron Servo-Hydraulic Test

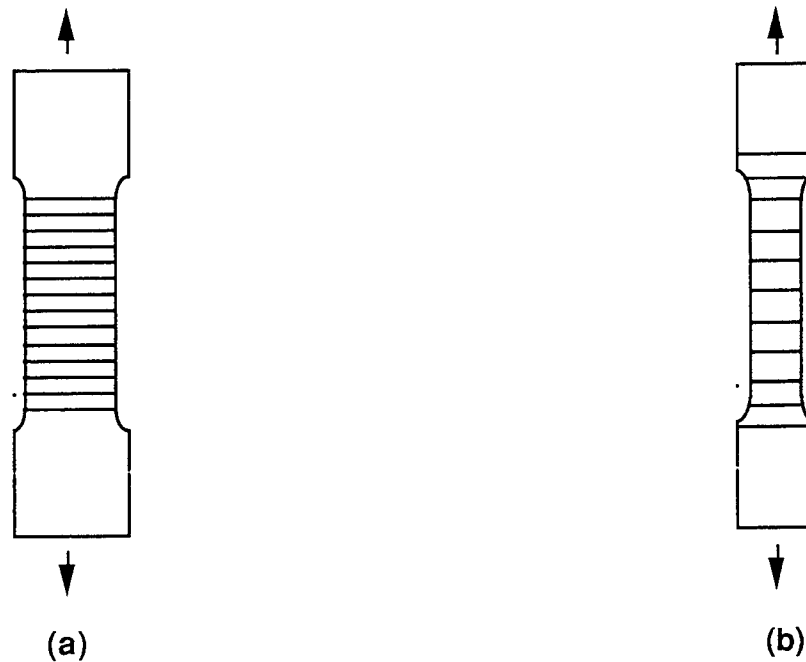


Fig. 2.1 Dumbbell specimen: a) Original material, b) Specimen cut from the drawn material.

System. The draw ratio was determined from the ratio of the spacing between the marked lines of the drawn (necked) material to that of the untransformed material. This ratio under draw stress is defined as λ_n and in the unloaded condition as λ_0 .

Thermal measurements

For thermal measurements of tensile experiments at 23 °C, an infrared microscope, a Model 600L IR Imaging Radiometer, capable of analyzing a spot size of 1 mm² with resolution 0.2 °C was employed. A very shallow notch was abraded into one edge of the tensile specimen to ensure the location of necking.

Dynamic mechanical Analyses

The thickness, width, and length of the specimens of the undrawn and drawn PC (molecular weight 29,000 g/mole) were 3.43 x 12.6 x 48.2 mm and 2.43 x 9.96 x 45.5 mm, respectively. The specimens were run in torsion and the temperature sweep modes on a Rheometrics 800-E mechanical spectrometer. The instrument software was RHIOS, version 3.01. The frequency of oscillation was 6.3 rad/s and the dynamic strain was 0.05 %. The specimens were loaded at room temperature, put under auto tension, then liquid-nitrogen cooled to -140 °C. The sample fixtures were then retightened to prevent sample slippage and the sample temperature equilibrated at -140 °C by holding for 15 minutes. The heating rate was set at 2 °C/min and the maximum temperature set to 200 °C.

2.3 Results

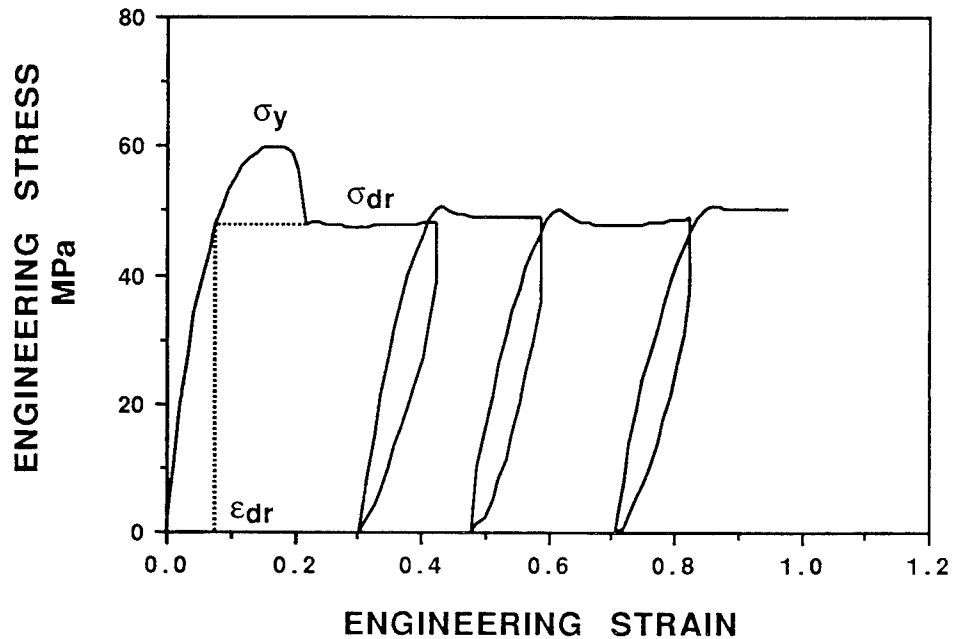


Fig. 2.2: The engineering stress-strain response for polycarbonate, PC, at 23 °C at an initial strain rate of $3 \times 10^{-4} \text{ s}^{-1}$.

Figure 2.2 shows the engineering stress-strain response for PC at 23 °C at an initial strain rate of $3 \times 10^{-4} \text{ s}^{-1}$. During the necking process the specimen was partially unloaded then reloaded to continue the necking. The engineering yield stress, σ_y , is taken as the maximum of the engineering stress at the low strains and is associated with the point at which a significant amount of microshear band formation has occurred [1,4,7]. On further strain the shear bands coalesce to form a well-defined zone or neck boundary. Necking is then observed to continue under essentially constant draw stress, labeled as σ_{dr} in the figure, by transformation of undrawn material to the drawn state across the neck boundary. The strain at which necking begins, ϵ_{dr} , is obtained by extrapolation of σ_{dr} to the engineering stress strain curve before σ_y . The partial unloading and reloading curves after yielding illustrates the initial recovery on unloading is fast, followed by a delayed recovery, as expected for a viscoelastic material. The subsequent reloading shows that a small amount of yielding occurs before neck growth continues as before unloading. The amount of yielding observed on reloading is proportional to the amount of strain recovery allowed in the specimen. Finally, as the neck propagates into the tab ends of the tensile specimen an upturn in the engineering stress is observed. The experimental data for the two molecular weight polycarbonates were indistinguishable in all respects except that the higher molecular weight PC reached a higher engineering stress before final fracture. Therefore, the tensile results of the two polycarbonates were combined.

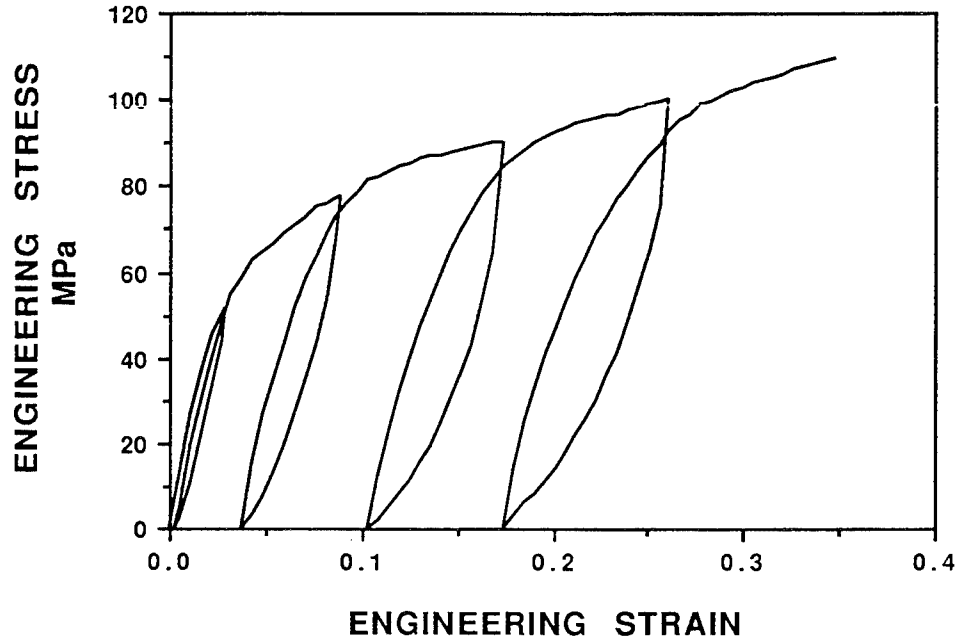


Fig. 2.3: The tensile behavior of the drawn PC.

The drawn PC was subjected to the same testing procedure. The results are illustrated in Figure 2.3. The tensile modulus of the drawn PC is higher than that of the undrawn PC by about 25 % and there is a significant change in the stress-strain response after loading beyond the initial true draw stress (the engineering draw stress corrected for the change in cross-sectional area, i.e., $\sigma_{dr}\lambda_n$). The unloading and reloading response of the drawn material is also shown in Figure 2.3, further exemplifying the change in stress-strain response above the stress at which it was originally unloaded.

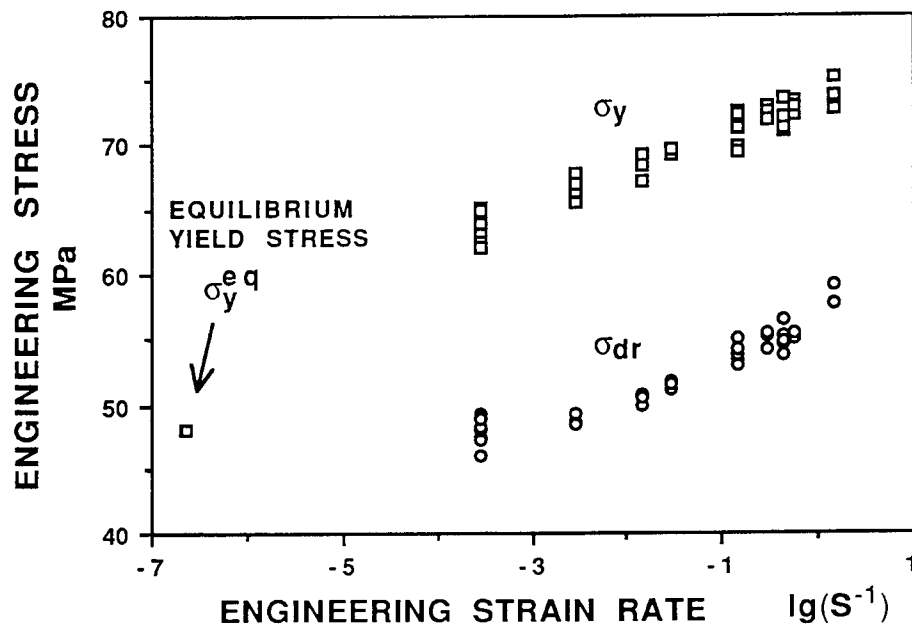


Fig. 2.4: Strain rate dependency of yield, σ_y , and draw stress, σ_{dr} at 23 °C.

Figure 2.4 shows the effect of strain rate on the values of σ_{dr} and σ_y for PC of thickness 0.7 mm. The dependency of σ_y on the logarithm of the initial strain rate has been examined [17]. To obtain very low strain rates the specimen were held at various constant loads and the strain rate taken simply as the reciprocal of the time to neck. Note that microcracking was observed below a constant stress of 48 MPa, whereas delayed yielding occurred at constant stress levels of 48 MPa and above. This phenomena was also described by Stokes and Bushko where the necking was observed to occur when the specimen had undergone an extension of about 6% strain [7]. Thus at 23 °C, the draw stress is assumed to level off at about 48 MPa at very low strain rates. We also call this value the equilibrium yield stress.

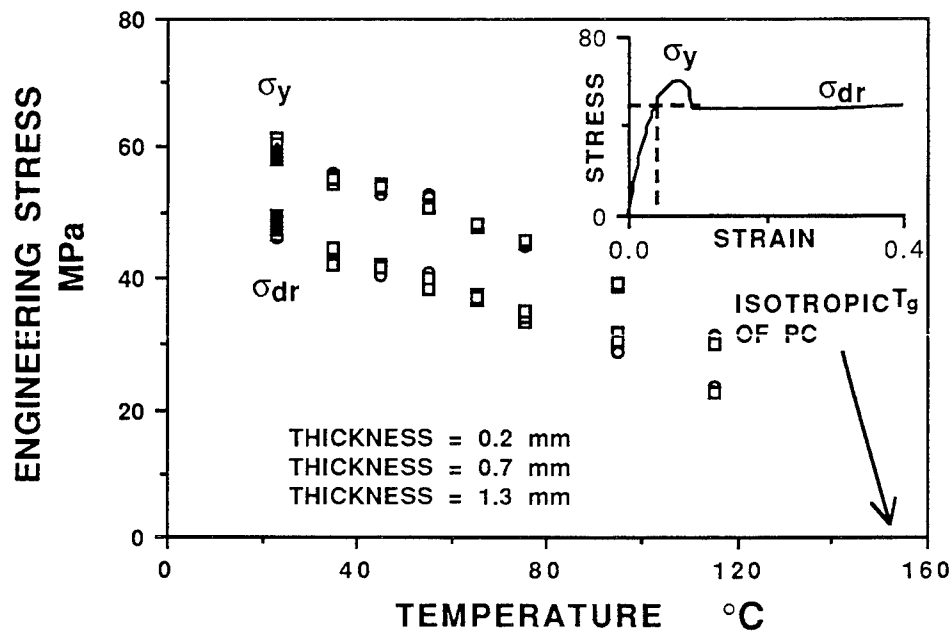


Fig. 2.5 Temperature dependence of σ_y and σ_{dr} at an initial strain rate of $3 \times 10^{-4} \text{ s}^{-1}$.

The effect of temperature on the tensile behavior of PC was examined with specimens pulled at the same initial strain rate of $3 \times 10^{-4} \text{ s}^{-1}$. Figure 2.5 shows that σ_{dr} and σ_y decay linearly with increasing temperature up to 115 $^{\circ}\text{C}$ and are independent of thickness within the range of thicknesses evaluated. At T_g the PC will not undergo necking behavior. The temperature dependency of ϵ_{dr} is shown in Figure 2.6 and the tensile modulus of the undrawn and drawn material are shown in Figure 2.7. The Poisson's ratio was determined at 25 $^{\circ}\text{C}$ using two extensometers during the tensile tests and found to be 0.395 and 0.433 for the undrawn and drawn PC, respectively.

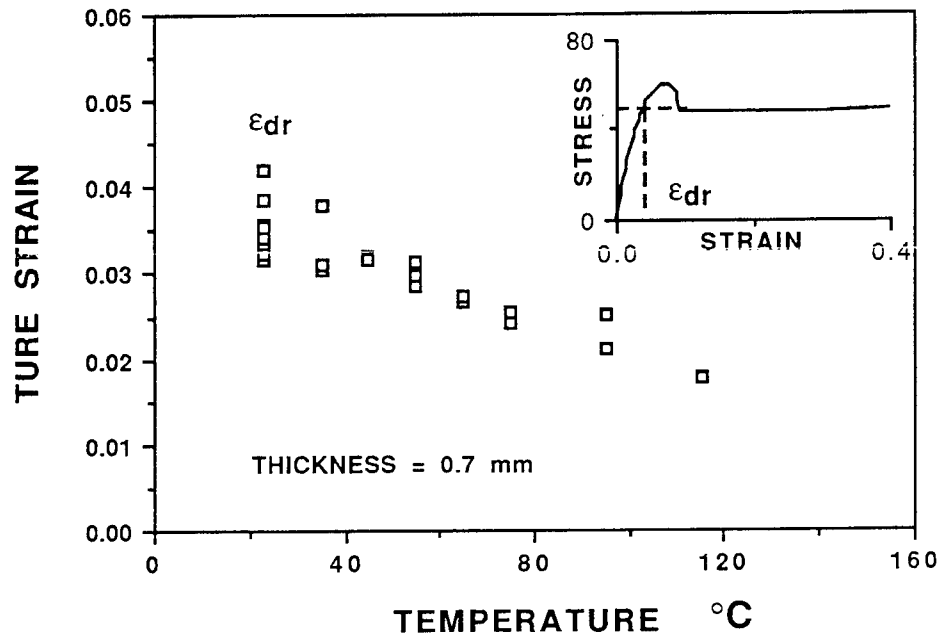


Fig. 2.6: Temperature dependence of the transition strain, ϵ_{dr} , at an initial strain rate of $3 \times 10^{-4} \text{ s}^{-1}$.

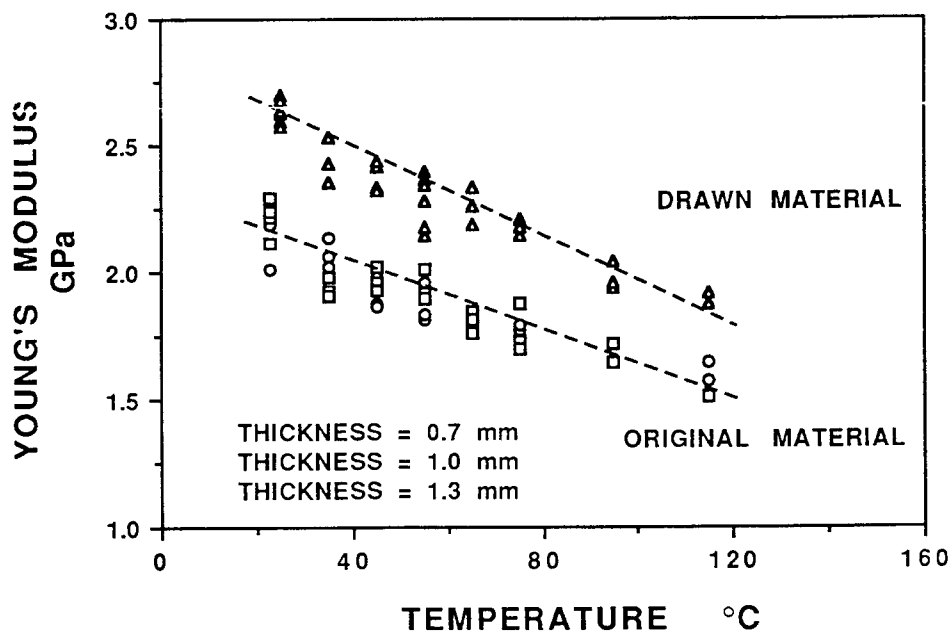


Fig. 2.7: Temperature dependence of Young's modulus, E , at an initial strain rate of $3 \times 10^{-4} \text{ s}^{-1}$.

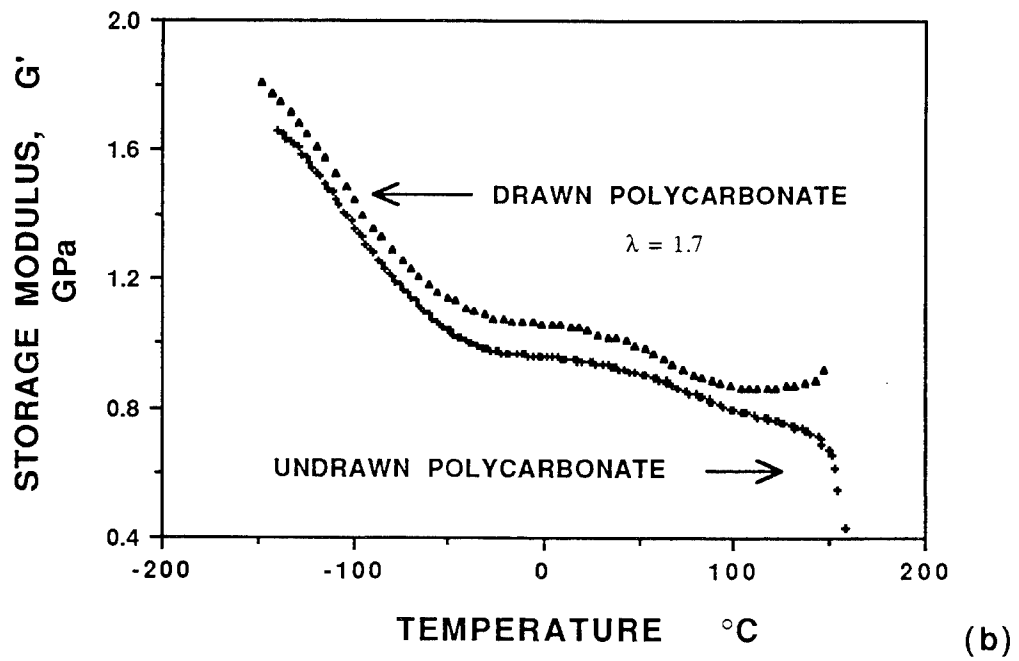
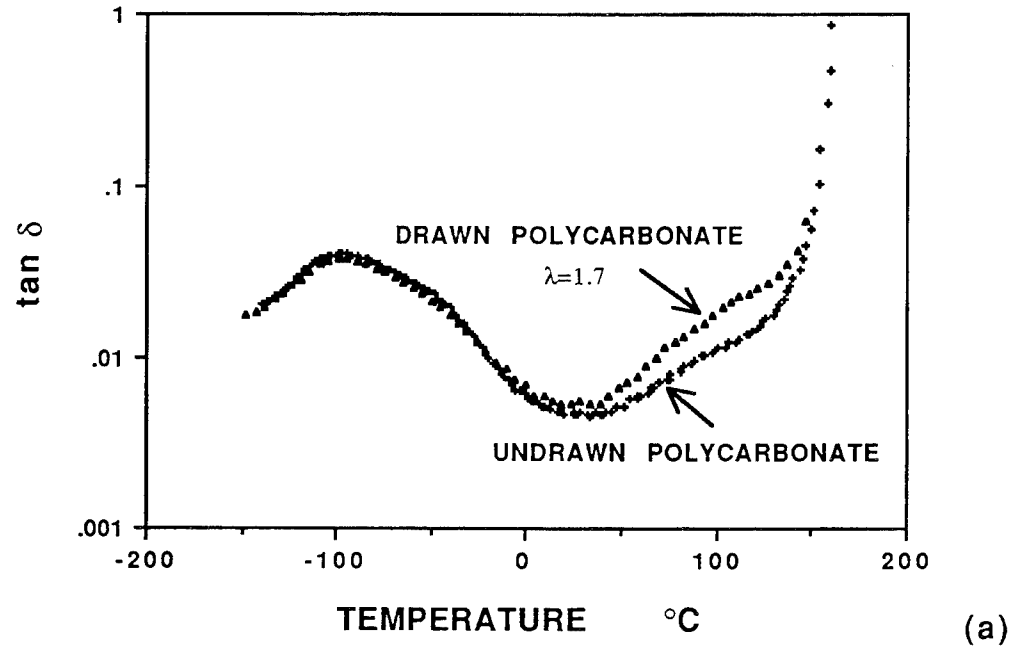


Fig. 2.8 Torsional dynamic mechanical analyses of the undrawn and drawn PC: a) Storage modulus G' , b) $\tan \delta$.

For complete characterization of the elastic properties and evaluation of the Poisson's ratio across a broad temperature range, the values of G' (the elastic portion of the shear modulus) and $\tan \delta$, as determined through the torsional dynamic mechanical analyses of the undrawn and drawn material ($\lambda_0 = 1.7$), are shown in Figure 2.8. As expected, the drawn material was found to have higher values of G' than the undrawn material. The values of the shear modulus of the drawn material exhibited an upturn above 90°C owing to material retracting. The retraction imposes more tensile stress on the sensor and results in higher calculated values. The retraction of the drawn material above 90°C is an

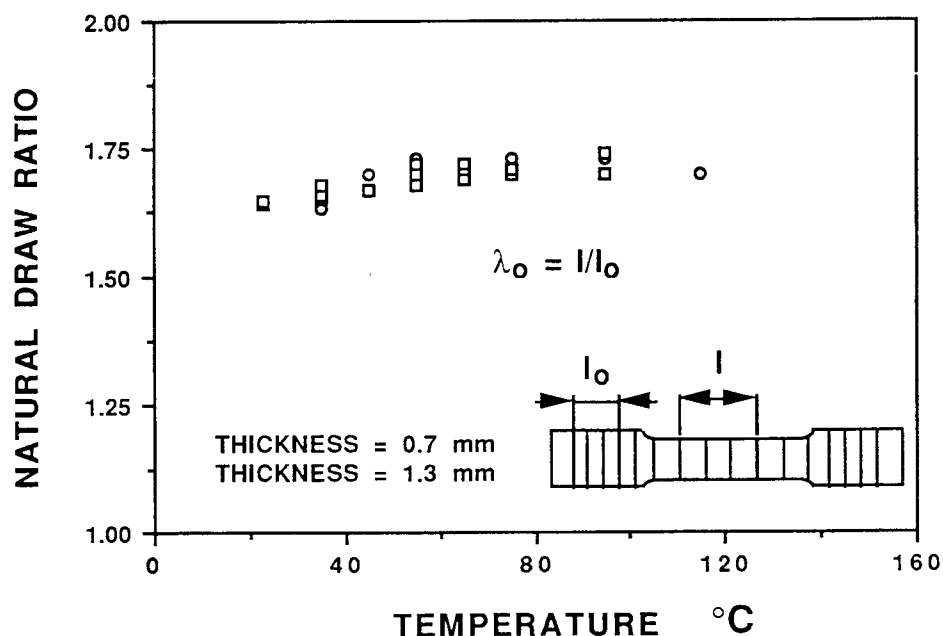


Fig. 2.9: Temperature dependence of the draw ratio λ_0 at an initial strain rate of $3 \times 10^{-4} \text{ s}^{-1}$.

indication of the relative increasing entropic contribution to the deformation. The Poisson's ratio for the undrawn and drawn material was found to change little with temperature in the range 25 to 90°C . The values of $\tan \delta$ for the

drawn material and undrawn material were essentially the same below $-25\text{ }^{\circ}\text{C}$, but the drawn material exhibited higher values above that temperature. This suggests that the local monomeric scale motions are little effected by the drawing process, but the larger scale segmental motions associated with the temperature regime above ambient temperature are strongly effected.

The weak temperature dependence of the draw ratio λ_0 of the unloaded necked PC is shown in Figure 2.9. Apparently λ_0 slightly increases from 1.65 to 1.72 over the temperature range $23\text{--}115\text{ }^{\circ}\text{C}$ and is essentially independent of thickness. The small increase in λ_0 may be caused by a small amount of creep as the specimens were observed to have a slightly higher value of λ_0 in the necked region where necking began than in the final region.

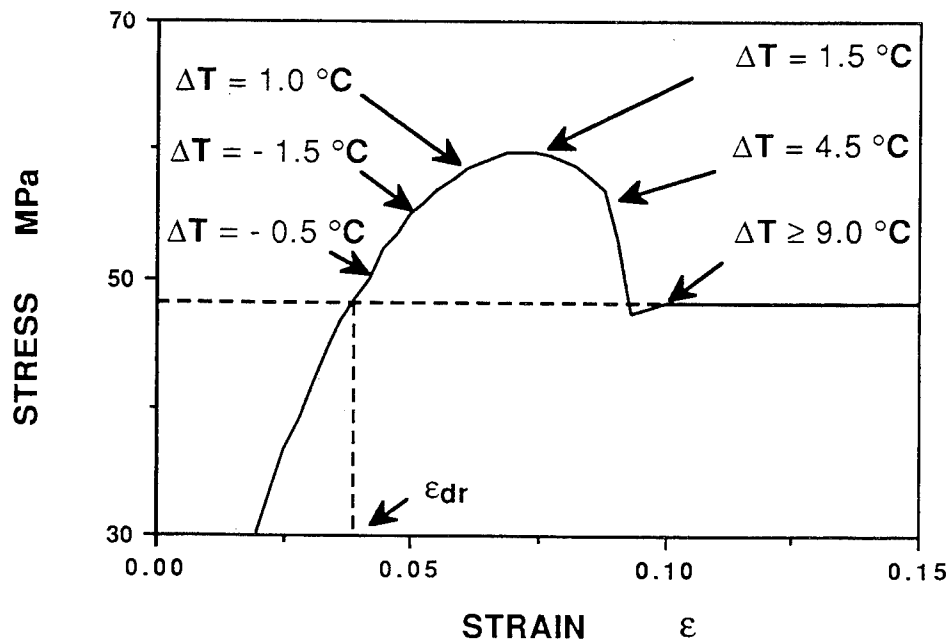


Fig. 2.10: Temperature changes during the necking of PC at $23\text{ }^{\circ}\text{C}$ and at an initial strain rate of $3 \times 10^{-4}\text{ s}^{-1}$.

Shown in Figure 2.10 is the differential surface temperatures recorded during the initial tensile deformation of PC at 23 °C and at an initial strain rate of $3 \times 10^{-4} \text{ s}^{-1}$. A temperature change was not observed within the resolution of the IR camera until the stress rose close to σ_{dr} . A temperature drop with a maximum difference of $-1.5 \text{ }^{\circ}\text{C}$ was then observed, followed rapidly by a change to an exotherm, coincident with multiple shear band formation. When the neck was fully developed a temperature increase of higher than $9 \text{ }^{\circ}\text{C}$ was observed. Figure 2.11 shows the thermomechanical behavior of the drawn material within the neck. On loading, a small reduction of temperature is first recorded up to the point where the stress exceeds $\sigma_{dr}\lambda_n$. Then an increase in temperature of about $5 \text{ }^{\circ}\text{C}$ is observed as the material undergoes further permanent drawing. On unloading a small temperature decrease of about $0.3 \text{ }^{\circ}\text{C}$ is observed. Repeated cycles reproduce the behavior described above.

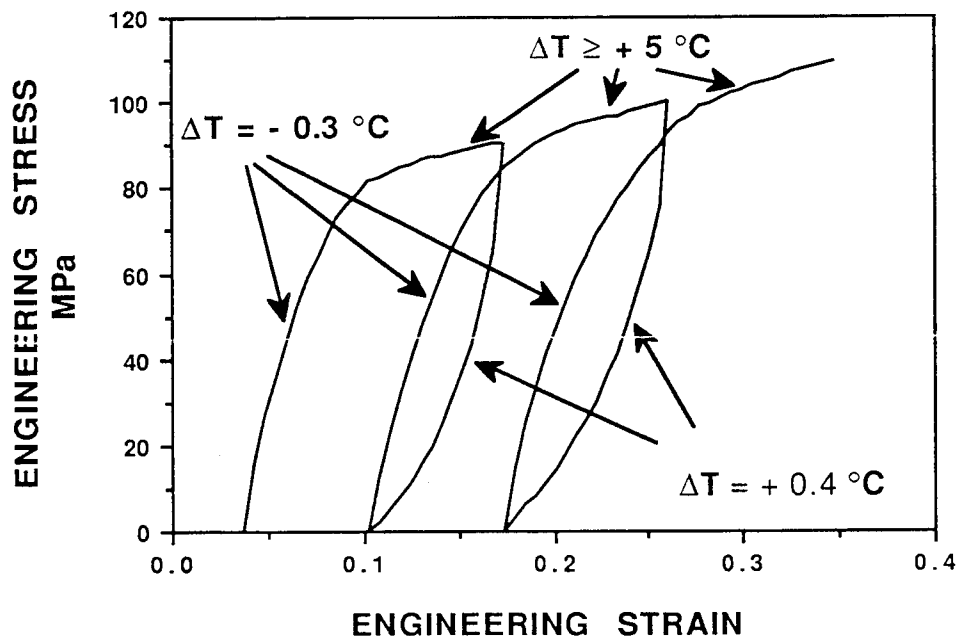


Fig. 2.11: Temperature changes on further stretching and unloading of oriented PC at 23 °C and initial strain rate of $3 \times 10^{-4} \text{ s}^{-1}$.

2.4 Discussion

It is important to consider the deformation of PC from a material particle perspective, in contrast to the geometry-dependent specimen response reflected in the engineering stress-strain curve. Most of the studies of large strain deformation have considered the necking of polymers from an external, or specimen standpoint [8]. In some studies, however, the mechanical behavior of material have been presented in the form of a true stress-strain curve [5,18]. Indeed, there are careful measurements by other researchers and by the authors that show that on necking the strain of the undrawn material on one side of the neck boundary suddenly decreases from ~ 1.06 to 1.03 , that is ϵ_{dr} , whereas in the drawn material the strain jumps to ~ 1.7 [7,18]. The natural draw ratio, λ_n is then calculated as $1.7/1.03$. The actual path dependency of the strain after

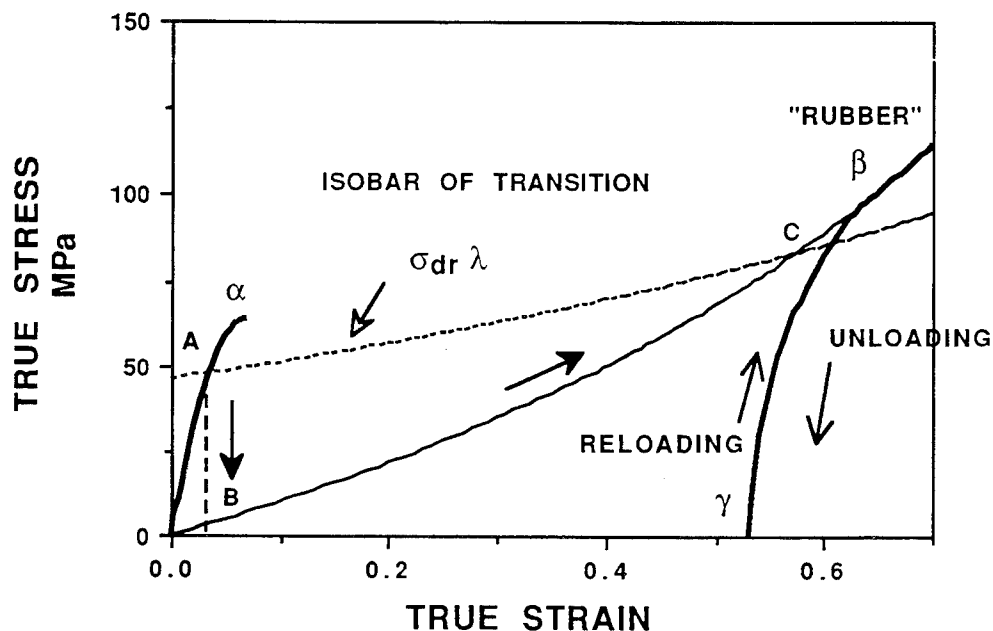


Fig. 2.12: The process of cold-drawing as transitions $\alpha \rightarrow \beta \rightarrow \gamma$.

yielding has not been determined. A reconstruction of the true stress-strain response for PC from a material particle perspective from the data shown in Figures 3 and 4, is given in Figure 2.12 in terms of the true stress, i.e., $\sigma_{\text{eng}} \lambda$, and the true strain, $\varepsilon = \ln \lambda$. Following conventional rubber elasticity, the true stress versus $\lambda^2 - 1/\lambda$ ($= e^{-2\varepsilon} - e^{-\varepsilon}$) is also considered.

$$\sigma_{\text{eng}} \lambda = G_p (\lambda^2 - 1/\lambda) \quad (1)$$

where G_p is the rubbery modulus. The stress-strain behavior of the undrawn and drawn materials are indicated by the solid lines, the dotted line A-C is the product of σ_{dr} and λ , and the dash-dot line B-C represents a deformation given by equation 1. Note that the stress-strain behavior of the drawn material above $\sigma_{\text{dr}} \lambda_n$ is coincident with $G_p (\lambda^2 - 1/\lambda)$ within our experimental observations.

The thermomechanical response of the initial and drawn PC can be used as a signature of its thermodynamic state. Indeed, an adiabatic small-strain tensile deformation results in cooling for a glassy polymer, and in heating in a rubber [19]. Thus, based on the observations presented in Figures 2.10 and 2.11, the cold-drawing behavior can be envisioned as follows. On extension, a point in the glassy unoriented material (α state) reaches ε_{dr} , then undergoes a transition to a rubbery mesostate β . The stress would immediately fall following the dashed line A-B since the transition time is much shorter than the rate of extension, i.e., essentially at constant strain. As the material particle should be in a mechanically balanced state, it would immediately stretch to a level of strain λ_n such that equation (1) is satisfied. The material particle would then remain at that value of the draw ratio (λ_n) as other undrawn regions of the PC are transformed into drawn material. Only when all the material is transformed can the material particle be stretched further by continuing along the B-C

deformation curve. On unloading the stretched material, the material particle transforms from the rubbery state to the oriented glassy state (γ state). The similarity of the temperature dependence of σ_{dr} and G_p for PC explains the observed constancy of draw ratio with temperature. This construct explains why the large tensile deformation of PC with necking did not follow the simple rubber elasticity treatment [5].

Thus, necking can be considered as a double glass transition. On application of stress, there is first an isotropic glass to isotropic rubber transition. Then, after stretching occurs through a rubbery mesostate, unloading involves transition from an oriented rubber to an oriented glass. The observed behavior of PC can be thought of as belonging to the class of "critical phenomena" such as with conventional phase transitions. A characteristic of critical phenomena is the discontinuity of a behavioral parameter (in this case true strain) with monotonic changes in the controlling factors, stress and temperature for this specific case of necking. This concept of the deformation of PC as a double glass transition reflects some aspects of previously considered models for yielding of amorphous thermoplastics [10-12] and is close to Haward's thoughts on rationalizing their observed large strain behavior [5]. Although the influence of the viscoelastic nature of the PC cannot be completely ignored, all the essential features of the true stress-strain response have been captured and should be applicable to other amorphous polymers that exhibit cold drawing. In the large tensile deformation of semicrystalline polymers with an isotropic T_g above the tensile test temperature, it is envisioned that the crystalline structure can contribute as a rigid filler to both the glassy and rubbery state, thereby increasing the draw stress and decreasing the natural draw ratio, as has been observed for poly(ether ether ketone) [5]. A full thermodynamic treatment of necking as a critical phenomena will be presented in a forthcoming paper.

2.5 Conclusions

1) The cold-drawing behavior of polycarbonate has been explained from a material particle perspective. The isothermal draw stress is shown to be a material parameter and the true stress-strain behavior of necked material above the true draw stress follows conventional treatment by rubber elasticity.

2) The cold-drawing behavior is considered to be a double glass transition. First as a transition from an isotropic glass to an isotropic rubbery state at yield. Then, on unloading after stretching of a rubbery mesophase as a transition from an oriented rubber to an oriented glass.

2.6 References

1. A. Kim, L.V. Garret, C.P. Bosnyak and A. Chudnovsky, *J. Appl. Polym. Sci.*, **49** 877 (1993)
2. T-J Chen, C.P. Bosnyak, C-I. Kao, and A. Chudnovsky, *J. Appl. Polym. Sci.*, **49** 1909 (1993)
3. K. Kadota and A. Chudnovsky, *Polym. Eng. Sci.*, **32** 1097, (1992)
4. M. Ma, K. Vijayan, A.S. Hiltner and E. Baer, *J. Mater. Sci.*, **24** 2687 (1989)
5. R.N. Haward, *Macromolecules*, **26** 5860 (1993)
6. N. Verheulpen-Heymans and J.C. Bauwens, *J. Mater. Sci.*, **11** 1 (1976)
7. V.K. Stokes and W. C. Bushko in *Use of Plastics and Plastic Composites: Materials and Mechanics Issues*, V.K. Stokes, ed., pp 1-21, MD-Vol 46, American Society of Mechanical Engineers, New York, 1993

8. B. Crist, *Plastic Deformation of Polymers*, to be published in *Materials Science and Technology*, Volume 12, E.L. Thomas, ed.; VCH, Weinheim, Germany.
9. F.H. Muller, *Kolloid Z.*, **114** 59 (1949)
10. G.M. Bryant, *Textile Research Journal*, **31** 399 (1961)
11. R.D. Andrews, and Y. Kazama, *J. Appl. Phys.*, **38** 4118 (1967)
12. C.P. Bosnyak, V. Krongauz, J.K. Rieke and A. Chudnovsky, *Papers of the Seventh International Conference, Deformation, Yield and Fracture of Polymers*, Churchill College, Cambridge, UK, 11-14 April, 1988, The Plastics and Rubber Institute, London.
13. S. Raha, and P.B. Bowden, *Polymer*, **13** 174 (1972)
14. J.W. Maher, R.N. Haward, and J.N. Hay, *J. Polym. Phys. Ed.*, **18** 2169 (1980)
15. R.N. Haward and G. Thackray, *Proc. Roy. Soc. A.*, **302** 453 (1968)
16. J.A. Koenen, B. Heise and H-G. Kilian, *J. Polym. Sci.*, Part B, Polym. Phys., **27** 1235-1260 (1989)
17. J.-C. Bauwens, *Polymer*, **25** 1523 (1984)
18. G. Buisson and K. Ravi-Chander, *Polymer*, **31** 2071, (1990)
19. Y.K. Govsky, *Thermophysical properties of Polymers*, Springer-Verlag, Berlin Heidelberg New York, 1992